Wear 432-433 (2019) 202965

Contents lists available at ScienceDirect

Wear

journal homepage: www.elsevier.com/locate/wear

Application of HVOF WC-Co-Cr coatings on the internal surface of small cylinders: Effect of internal diameter on the wear resistance

J. Pulsford[a], F. Venturi[a], Z. Pala[b], S. Kamnis[c,**], T. Hussain[a,*]

[a] Faculty of Engineering, University of Nottingham, Nottingham, NG7 2RD, UK
[b] GE Aviation, Beranovych 65, Prague, Czech Republic
[c] Castolin Eutectic -Monitor Coatings Ltd, North Shields, NE29 8SE, UK

ARTICLE INFO

Keywords:
HVOF
ID spray
Wear
WC-Co-Cr
Thermal spray

ABSTRACT

Due to the restrictions and mediocre performance of current methods of coating complex shaped parts in which line of sight processes currently struggle, the development of new coating methods is essential, with High Velocity Oxy-Fuel (HVOF) thermal spray coatings being a good candidate. In this study, a new compact High Velocity Oxy-Air Fuel (HVOAF) thermal spray torch designed to coat internal surfaces was traversed within cylindrical pipes of internal diameters (IDs) of 70 mm, 90 mm and 110 mm and a WC-10Co-4Cr coating was applied with a commercially available powder feedstock. Powder and coating microstructures were analysed using SEM/EDX and XRD. Fracture toughness and microhardness of the coatings were measured, and dry sliding wear performance was investigated at two loads: 96 and 240 N. It was found that the coating sprayed at 90 mm (medium ID) had a lower specific wear rates at both test loads due to the highest fracture toughness and microhardness; whereas, the coating sprayed at 110 mm (high ID) showed the highest specific wear rates at both low and high conditions due to poor fracture toughness.

1. Introduction

The development of an alternative method of coating complex-shaped parts in which line of sight processes are limited is currently essential, due to the regulatory limitations (REACH legislation, Regulation (EC) No. 1907/2006) restricting the use of currently used methods such as electroplated hard chrome (EHC). High velocity oxy-fuel (HVOF) thermal sprayed coatings have been proposed as a good alternative to electroplated hard chrome as they are more environmentally friendly, better performing and more flexible in terms of the choice of coating materials available [1]. In particular, cermet materials sprayed by HVOF such as WC-Co-Cr may be suitable to replace EHC coatings for applications in which resistance to sliding wear is required, due to the fact that these coatings have been shown to offer superior wear resistance [2]. As a result, a number of industrial sectors such as aerospace, off-shore oil and steel production [3,4] have been searching for a way to apply thermal spray coatings on complex shaped parts traditionally processed using EHC.

The line of sight nature of thermal spray processes prevented their use in many applications, such as coating internal surfaces and complex shaped parts, due to the large dimensions and stand-off distance required. In order to mitigate these limitations, a new generation of thermal spray systems have been developed, in the form of spray torches with much smaller dimensions able to fit in narrower spaces andeffectively coat surfaces at much shorter stand-off distances [5]. This potentially enables the use of thermal spraying to coat internal surfaces in which non-line of sight processes like EHC were once required. However, using a spray torch with a short barrel at smaller stand-off distances produces new challenges to overcome, for instance the temperature of in-flight particles has been shown to be strongly dependant on the length of the barrel [6]. Consecutively, spraying at smaller stand-off distances may mean the in-flight particles are still undergoing acceleration and heating when impacting the substrate [7,8]. Combining these two effects may result in a poor coating, due to the fact the particles may have not melted sufficiently alongside impacting the substrate at a relatively low velocity, resulting in insufficient plastic deformation and low adiabatic shear instabilities [9]. Finer powder feedstocks in particular may be more suitable than larger powders when spraying at these conditions, as smaller particles with a lower mass will accelerate at a faster rate and require less energy to reach their optimum temperature in comparison to larger, heavier particles of the same material. Also, smaller particles have a higher surface area to

* Corresponding author.
** Corresponding author.
E-mail addresses: spyros@monitorcoatings.com (S. Kamnis), tanvir.hussain@nottingham.ac.uk (T. Hussain).

https://doi.org/10.1016/j.wear.2019.202965
Received 26 November 2018; Received in revised form 25 April 2019; Accepted 10 July 2019
Available online 11 July 2019

volume ratio which favours heat transfer from the hot environment. However, when spraying WC based cermet materials, it has been shown in previous work that reducing the particle size can make the WC phase more susceptible to decomposition, which for carbides is referred to as decarburisation [10]. This effect arises due to the WC grains dissolving in the molten binder phase, after which carbon will begin to be removed by reacting with oxygen at the gas-liquid interface [11]. Therefore, this mechanism is strongly linked to particle temperature and, as finer powder particles with a lower mass require less energy to heat up in comparison to larger heavier ones, they are also more vulnerable to overheating [12]. Careful spray parameter optimisation and powder feedstock selection is needed to give rise to sufficient particle velocity to achieve a viable coating, meanwhile preventing overheating of the particles to prevent decarburisation. The coating of the surfaces inside of parts with internal diameters larger than 125 mm by HVOF ID technology has begun to be more widely accepted as the development of this field continues. However, applying coatings using HVOF thermal spray using commercial feedstock powders within IDs less than this length, in particular IDs of 100 mm or less, has been challenging due to the previously mentioned issues. Currently little is known about the performance of HVOF coatings sprayed within cylinders with a small internal diameter; however this work presents data regarding the microstructure, mechanical properties and sliding wear resistance of coatings sprayed at IDs as low as 70 mm. In this study, a compact HVOAF spray system capable of operating with a mixture of air and fuel gases developed by Castolin Eutectic-Monitor Coatings Ltd. (North Shields, UK) [13] was mounted within pipes with internal diameters of 70 mm, 90 mm and 110 mm and used to apply a WC-10Co-4Cr coating. The coatings microstructure and the associated mechanical properties were studied with SEM and XRD to determine the effect of the changing internal diameter on each coating. Unlubricated sliding wear testing against a WC-Co counterbody was used to study the effect of changing ID on the coating's sliding wear resistance and as a means to test the performance of the three coatings. The aim of this work is to demonstrate that WC-Co-Cr HVOF thermal sprayed coatings with useful tribological properties can be applied on internal surfaces within cylinders of IDs as low as 70 mm, as well as showing the potential effect of how changing the internal diameter affects these properties in order to assist future spray parameters optimisation. Wear testing was carried out at two separate loads to simulate low and high load applications.

2. Experimental

2.1. Deposition of internally sprayed coatings

38.1 mm diameter x 6 mm discs of 416 stainless steel (12–14% Cr, 1.25% Mn, 0.15% C, 0.15% S, 0.6% Mo, 0.06% P, 1% Si in weight %) were mounted using magnets on the inside of three cylindrical tubes that, taking into account the disc and magnet thickness, correspond to spraying on cylindrical tubes with internal diameters of 70 mm, 90 mm and 110 mm. The samples obtained will be referred to with the names ID70, ID90 and ID110 throughout the text, and correspond to actual stand-off distances of 30 mm, 50 mm and 70 mm, respectively. The axial length of pipe used was 200 mm. A photograph of the setup is shown in Fig. 1.

A compact HVOAF spray system developed by Monitor Coatings—Castolin Eutectic, designed to coat internal surfaces, was used to deposit the coatings. The torch uses a mixture of hydrogen (200–300 SLPM), air (100–400 SLPM) and oxygen (100–200 SLPM) depending on the mode of operation. The combustion chamber pressure was 6–8 bar. The gun was positioned inside the pipe and moved vertically at 2 mm/s and the substrate was rotated around it as shown in Fig. 1. In order to monitor the temperature of the part being sprayed, an external thermal imaging camera was used. To prevent overheating of the pipe the rotational speed of the part could be increased, thereby reducing the time the part is exposed to the flame for each pass. Air is also blown into the cylinder to assist cooling and help the removal of undeposited particles. Fixed spray parameters were used when spraying each ID. The feedstock powder used in the study was a commercially bought powder (H. C. Starck, Munich, Germany), stated by the manufacturer to have a particle size range of – 15 + 5 μm and a medium WC grain size. Details about the feedstock powder are shown in Table 1. The stainless steel discs were cleaned and grit blasted prior to coating deposition, with the spray parameters developed from previous optimisation studies [10].

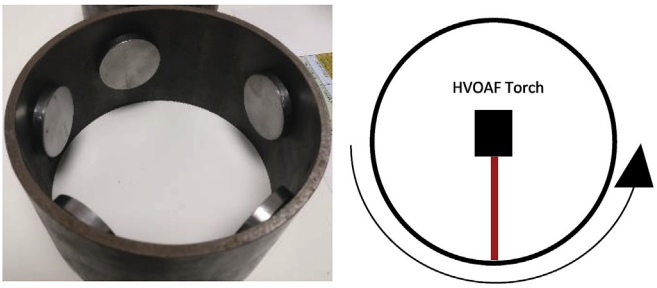

Fig. 1. Photograph and plan view schematic of ID coating deposition setup (drawing not to scale). The torch was fixed in x and y directions and the pipe holding the substrates rotated during deposition.

2.2. Dry sliding wear testing

Unlubricated sliding wear testing was carried out at room temperature (≈25 °C, relative humidity ≈ 60%) using a conventional ball on disc apparatus, shown schematically in Fig. 2, following the instructions described by the ASTM G99 standard [14], against a 94% WC – 6% Co (wt.%) ball with a diameter of 9.5 mm (Dejay Ltd, Launceston, UK) that was replaced at the end of each test. Uninterrupted wear tests with a sliding speed of 0.05 m/s and distance of 500 m were run at loads of 96 N and 240 N, with these conditions chosen with the aim of promoting wear of the coating surface and to follow on from previous work [10]. The coefficient of friction was monitored throughout the test using a LVDT (linear variable differential transformer). The top surfaces of the coatings were polished to a 1 μm finish and were cleaned with IMS (Industrial methylated spirit) prior to wear testing. 2 separate samples were subjected to wear testing for each coating at both loads.

The volume loss of each disc was determined using the profilometry method used in other studies [10]. A surface profiler (Taylor Hobson Ltd, Leicester, UK) was used to measure 4 line traces perpendicular to the sliding direction to determine the cross sectional area of the wear track. These values were averaged and then multiplied by the track length to estimate the total volume of material removed during the wear test. The specific wear rate could then be calculated by dividing the total volume of material lost by the product of the load and sliding distance. The wear of the WC-Co counterbody during the test resulted in a near flat surface.

The morphology of the wear scar and fracture mechanisms were then examined in plan view using a scanning electron microscope (Jeol 6490LV, Jeol Ltd., Japan), with optical microscopy (Nikon Eclipse LV100ND, Nikon, Japan) used to image the WC-Co counterbody. Cross sections of the wear scars were also imaged using SEM with secondary electrons (SE) imaging with the samples being sectioned using a SiC cutting disk and mounted in a cold mounting resin to ensure the preservation of important delicate features.

2.3. Coating characterisation

Coating cross sections were prepared by sectioning the sample using a SiC cutting wheel in a precision cutting saw. Powder and coating sections were then mounted in a conductive mounting compound (Metprep Ltd, UK), ground with SiC papers down to a 15.3 μm grit size

Table 1
Feedstock powder characteristics (size ranges and chemical compositions) as supplied by the manufacturer.

Powder Commercial Designation	Chemical Composition (wt. %)						Size range (μm)	
AMPERIT® 554.067	W	Co	Cr	C	O	Fe	D90	D10
	Balance	8.5–11.5	3.0–5.0	5.0–6.0	Max 0.2	Max 0.6	18–24	5–8

and then polished down to a 1 μm finish. The feedstock powder, coating cross sections and wear tracks were imaged using a scanning electron microscope (Jeol 6490LV, Jeol Ltd, Japan), utilising both SE imaging and back scattered electron (BSE) imaging. X-ray diffraction was performed on the feedstock powder and coating top surfaces using a Siemens D500 with Cu *Kα* radiation (1.5406 Å) in the $20^\circ \leq 2\theta \leq 90^\circ$ range to identify the phases present in the powders and coatings. A step size of 0.02° and dwell time of 3 s were used. Quantitative Rietveld refinement was carried out using TOPAS (Coelho Software, Australia) to determine the phase composition within the feedstock powders and coating samples.

The microhardness of the coatings was measured on polished cross-sections by using a Vickers microhardness indenter (Buehler, Illinois, USA) at a load of 300 gf and a dwell time of 10 s; for each sample 10 indentations were made in the centre of the coatings running parallel with the substrate. Fracture toughness of the coatings was measured by indenting on polished cross sections with a 2.5 kgf load and measuring the crack lengths parallel to the substrate using optical microscopy; cracks propagating from the left and right tips of the indent were considered. The fracture toughness K_Ic was determined using the method described by Evans and Wilshaw [15], shown in equation (1):

$$K_{Ic} = 0.079\left(\frac{P}{a^{3/2}}\right)\log\left(\frac{4.5a}{c}\right) \quad (1)$$

Where P is the applied indentation load, a is the indentation half diagonal and c is the crack length from the indent centre. This expression is only valid when $0.6 \leq c/a \leq 4.5$; all measurements of c and a were determined to fit within this range. 10 indents were measured for each coating, and the mean and standard deviation of the results is presented.

3. Results

3.1. Microstructural characterisation of coatings

The XRD spectra, shown with the results of the quantitative Rietveld refinement of the feedstock powder and the three sprayed coatings, are displayed in Fig. 3. The phases detected in the feedstock powder consist of the primary WC phase, η-phase carbide, Co_6W_6C and a solid solution of (Co,Cr). Rietveld refinement was unable to give a conclusive answer on whether the (Co, Cr) solid solution found within the powder feedstock has an fcc or hcp crystal structure, as Rietveld scores were comparable.

All three coating spectra show that some carbon loss occurred during the spray process, as expected, due to the emergence of the W_2C phase. A right hand shoulder on the W_2C peak positioned at $2\theta \approx 40^\circ$ can be seen on all coating scans, and this can be attributed to the (422) peak of Co_3W_3C positioned at $2\theta = 40.588^\circ$ according to PDF–01-078-5005. Using the Rietveld refinement method it was determined that the W_2C content of ID70 coating (6.76 wt % W_2C) was slightly less than the ID90 coating (6.81 wt % W_2C). However, ID110 was found to contain a lower weight percentage of W_2C than the other two coatings, with a calculated weight composition of 4.68%. To compensate for the lower amount of this phase in ID110, a greater weight percentage of η-phase carbide M_6C was found in this coating compared to the other two. The diffraction peaks within the $2\theta = 37^\circ$–46° range have been noted to have broadened slightly in comparison to the feedstock powder spectrum. This may indicate that some amorphous material formed during the spray process due to the elevated temperatures.

SEM images of the feedstock powder and powder cross section are presented in Fig. 4. The powder particles have an angular shape typical of sintered and crushed powder feedstocks with little intra particle porosity. Low and higher magnification BSE SEM images of the three coatings are shown in Fig. 5. The thickness of ID70, ID90 and ID110 were measured in 4 different locations and averaged, resulting to be (224 ± 7) μm, (214 ± 7) μm and (129 ± 4) μm respectively. Spray parameters, RPM of the part and gun vertical movement speed were kept constant when spraying all three coatings, so the actual linear speed with which the substrate is moving relative to the torch will differ, possibly contributing to this thickness difference. Throughout the microstructure of all three coatings, the presence of a phase with a darker contrast is observed in Fig. 5a, c and e.

An EDX point scan was undertaken on such a site (marked by the red dot on Fig. 5a) and the composition was found to consist mostly of Fe, with trace amounts of Si and Mn, suggesting it originated from the 416 stainless steel substrate as no traces of these elements were found within the powder feedstock. The presence of these substrate impurities appears to be most visible within the microstructure of ID70, implying that the shorter stand-off distance required to spray the smaller internal diameter may be to blame. These Fe particles are likely to be an artefact of spraying inside a pipe where any loose debris will be attracted to the coating because of the mounting magnets.

The high magnification BSE images reveal a complex microstructure, typical of a cermet coating. Grains of WC, appearing as the brightest phase, due to the mean atomic number in the BSE image, can be seen distributed throughout surrounded by a binder phase with a varying contrast. The varying contrast of the binder phase is an

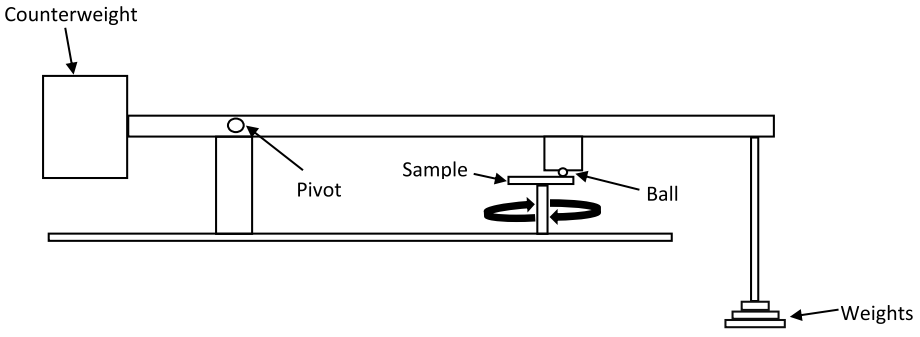

Fig. 2. Schematic of the ball on disc tribometer.

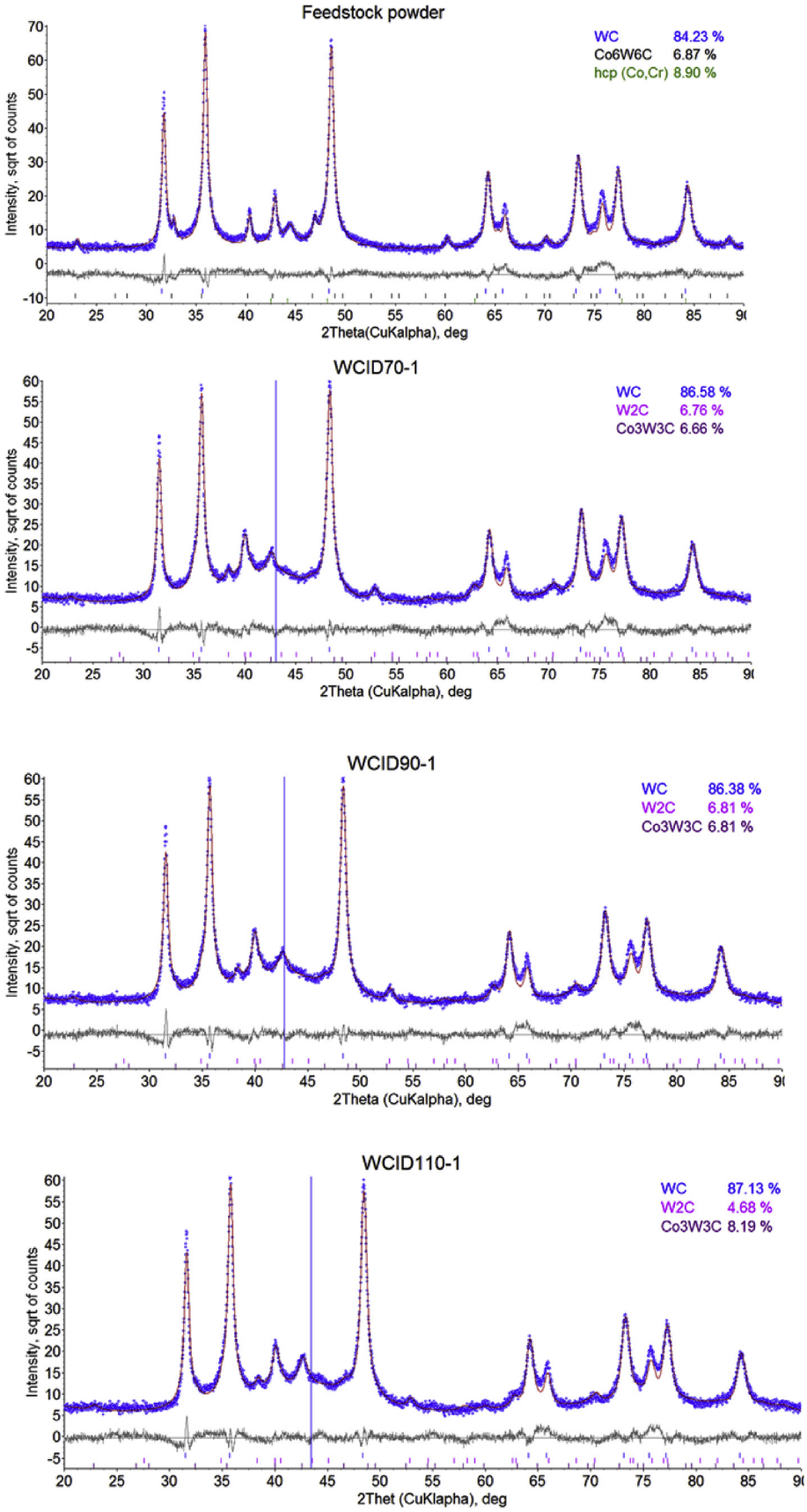

Fig. 3. XRD spectra of the three sprayed coatings and feedstock powder. The blue dots represent the measured data, Rietveld fit is shown by the red line and the blue vertical line corresponds to the maximum of split Pearson VII function that models the halo from amorphous phase(s). The quantities are shown in wt. %. The feedstock powder mainly contained WC, $M_{12}C$ carbides alongside a solid solution of hcp (Co, Cr). The coatings can be seen to contain W_2C and M_6C carbides. Between $2\theta = 37°–46°$ a slight broadened region can be observed on the 3 coating spectra possibly indicating amorphous material. The peak positions can be seen from the coloured marks below the scans – WC, W_2C and eta carbide phase peak positions are top, middle and bottom respectively. (For interpretation of the references to colour in this figure legend, the reader is referred to the Web version of this article.)

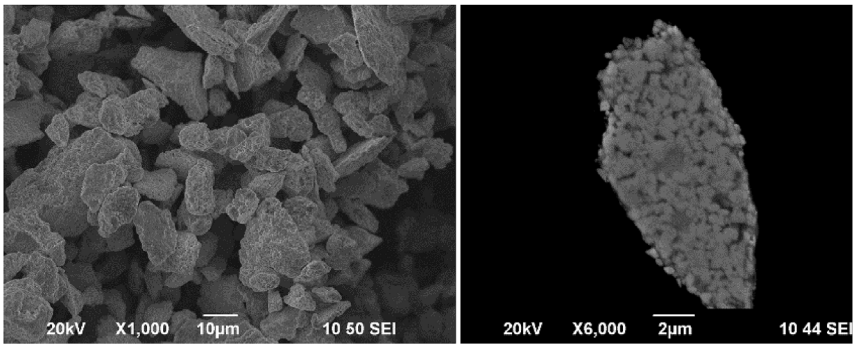

Fig. 4. SE SEM images of feedstock powder showing blocky, angular morphology and polished cross-section of the powder showing WC particle in a CoCr matrix.

indication of tungsten dissolution into the binder phase, suggesting that particles were well melted by the torch prior to impacting the substrate.

The Vickers microhardness and indentation fracture toughness of the three coatings is presented in Table 2. ID70 was found to have the lowest microhardness out of the three coatings, with the values measured during these tests also having the highest standard deviation suggesting a larger degree of non-homogeneity in terms of the microhardness throughout this coating in comparison with the others. ID90 was found to have the highest microhardness and fracture toughness of

Table 2
Microhardness and indentation fracture toughness measured on the polished cross-section of three coatings. The table shows average values with standard deviation.

Sample	Vickers Microhardness (300gf)	Fracture toughness K_{Ic} (MPa.m$^{0.5}$)
ID70	1201 ± 106	3.92 ± 0.36
ID90	1319 ± 40	4.82 ± 0.24
ID110	1310 ± 52	3.34 ± 0.52

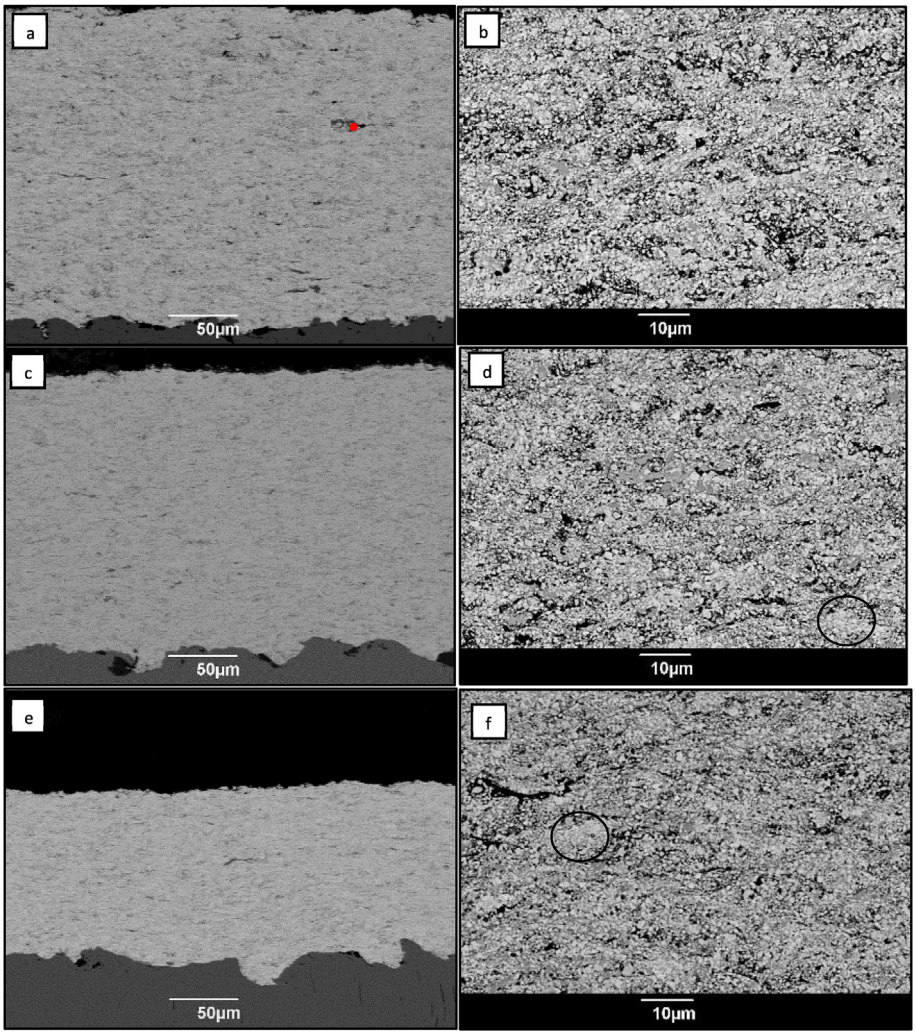

Fig. 5. Low (left column) and high magnification (right column) BSE SE images of the three coatings with (a–b) ID70, (c–d) ID90, (e–f) ID110. An EDX spot scan was performed at the position marked on Fig. 5a with the results available in the text. The WC grains (bright grey) are surrounded by a binder phase of various contrast levels (grey, black areas). Areas where WC has partially dissolved in the surrounding binder are circled.

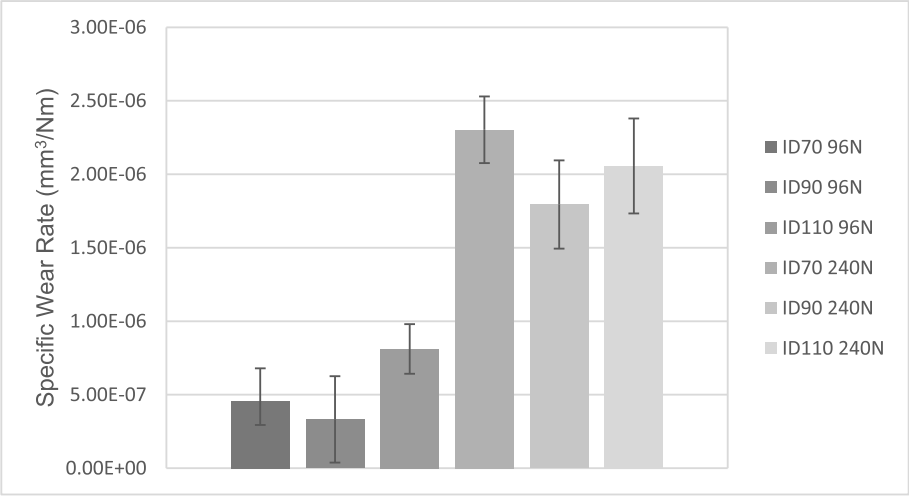

Fig. 6. Specific wear rates of the three coatings at 96 N and 240 N with error bars showing the total range of values measured.

all three coatings measured, with the standard deviation of the measured values being the smallest, suggesting a more homogenous microstructure. The microhardness of the ID110 coating is comparable to the harder ID90, however the fracture toughness of this coating was found to be lowest of the three coatings.

3.2. Dry sliding wear testing

The measured specific wear rates of the three coatings tested are presented in Fig. 6. At 96 N ID90 shows the lowest wear, with ID110 wearing out the most. At this load, the wear of all three coatings is in the 10^{-7} mm^3/Nm range, meaning the amount of material loss is small. At the 240 N load, ID90 again shows the lowest wear, with ID70 performing the worst. From analysing the relationship between the measured specific wear rates of ID70 and ID90, it appears that both coatings reacted to the increase in load in a similar manner. However ID110 did not fit this trend, suggesting a different mechanism of wear may be taking place in this coating in comparison to the others.

In order to gain an understanding of the wear mechanisms taking place during the sliding wear test, the wear tracks were analysed using SEM. Images of the plan view of the wear scars formed from the 96 N tests are displayed in Fig. 7. Different magnifications of the wear tracks have been used in this figure to highlight the specific features on the sample surface. On the ID70 sample, isolated areas deficient of the WC hard phase are visible. This brittle phase was found in a previous study and was shown by EDX analysis to contain W = 64.7 wt%, O = 26.4 wt %, Co = 4.9%, C = 3% and Cr = 1% [10]; with this tungsten oxide phase probably formed by tribo-oxidation. Cracks are seen propagating across the wear track perpendicular to the direction of counterbody movement on the ID70 sample at 96 N, covering many splats at a time. At the same load, these cracks cannot be seen on the ID90 sample. The surface of the ID90 wear track is covered with micron sized pores; likely in sites where WC phase pull-out has occurred.

The wear scar of the ID110 sample at the 96 N load can be seen to have suffered a greater amount of material loss in comparison to the other two coatings at this load, due to many large sites of material pull-out being visible. Unlike the ID90 coating, the size of these pull-out sites was found to be many times larger, with an example displayed in the high magnification image being at least 50 μm in diameter. Alongside the main hole, other areas showing signs of cracks can also be observed. It should also be noted that the wear track of the ID110 sample is also much wider compared to ID90 under the same loading condition. The friction coefficients for the 3 coatings at 96 N all are found to settle between 0.3 and 0.4 for ID70, and 0.5–0.6 for ID90 and ID110 after an initial breaking in period.

The wear tracks of the samples tested at 240 N are shown in Fig. 8. ID70 and ID90 show similar mechanisms of wear, with visible brittle areas of the tungsten oxide observed; these oxides appear darker in the BSE images. The wear scar of the ID110 sample at 240 N was found to have cracks propagating from the edge of the track parallel to the counterbody movement direction; these then curve into the track centre at some locations. These cracks were shown to propagate in particular through the brittle binder. Such extensive cracking was only seen in ID110 coating at the higher load. It should be noted that the width of the track is relatively narrower in this sample compared to the rest under the same load. The friction coefficient of the ID70 and ID90 samples at 240 N is seen to rise to a peak value between 0.7 and 0.8.

More information on the wear mechanisms taking place can be uncovered by analysing the cross section of the wear tracks by SEM, shown in Fig. 9 at both 96 N and 240 N. The samples were cut across the worn surface, perpendicular to the direction in which the counterbody travelled. The cross section of the ID70 and ID90 samples show a similar scar shape at both loads, further suggesting the same mechanism of wear is taking place when load is increased. These samples showed no evidence of sub surface cracking beneath the worn surface, suggesting good inter-particle bonding in these coatings. Conversely, the cross sectional SEM images of the ID110 worn surface at both loads show severe sub surface cracking, with the cracks propagating into the coating centre, roughly parallel with the substrate. Lower magnification images were chosen here to show the overall coating thickness and the nature of these cracks. The extensive damage to the coating microstructure is in line with the volume loss measurements, the wear tracks are much deeper and the cracks propagated from the bottom of the removed material. A similar phenomenon is also observed in the ID110 coating at higher load.

4. Discussion

The feedstock powder is found to contain WC, $M_{12}C$ (Co_6W_6C) and hcp (Co, Cr) phases and the hcp phase could not be detected (XRD detection limit 1–2 wt%) in all three coatings. The XRD spectra reveal that the W_2C is present in all three coatings but not in the powder feedstock, indicating that some carbon loss is occurring during spraying and that particle temperatures were sufficient to allow some degree of binder phase melting. The presence of peak broadening in the region $2\theta = 37°–46°$ on all coating spectra have been shown by others to possibly indicate the presence of amorphous or nanostructured material [16]. It is interesting to note that in all three coatings M_6C (Co_3W_3C) carbide was detected instead of $M_{12}C$, which was present in the original powder feedstock. Rietveld refinement uncovered some differences in

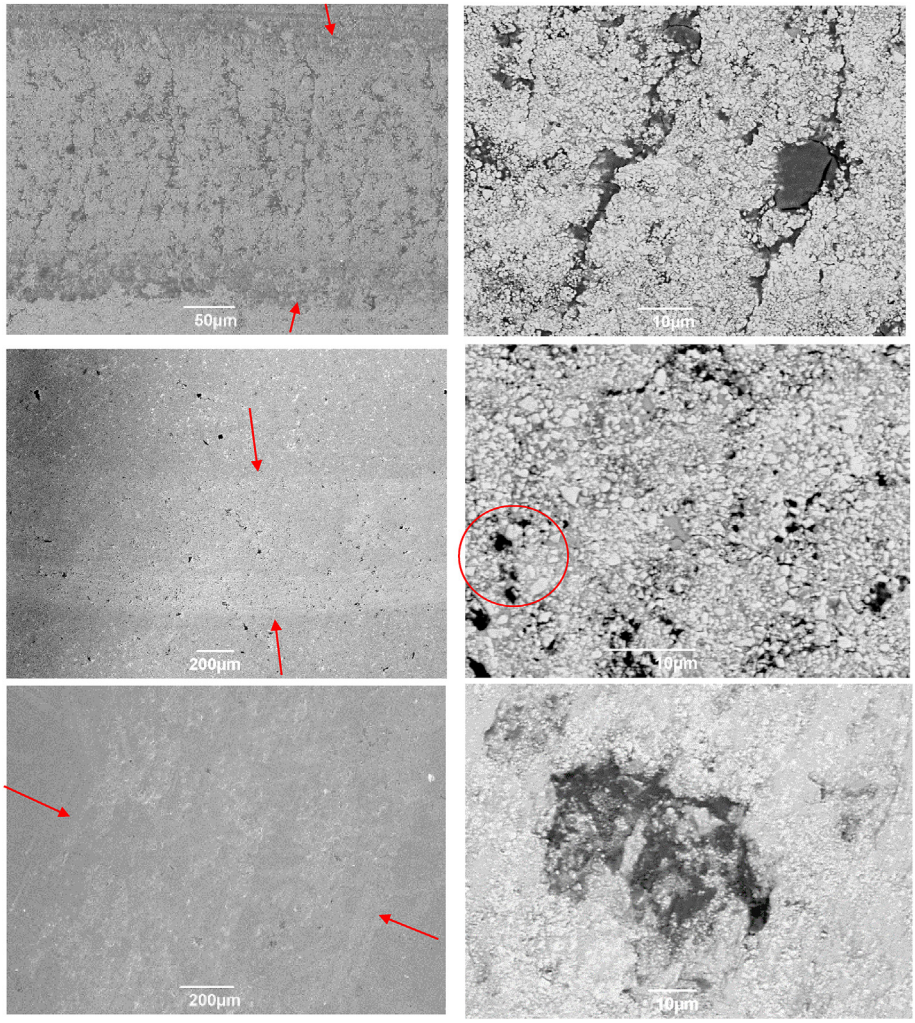

Fig. 7. Plan view SEM SE images of the wear scars produced from the sliding wear tests at 96 N. The position of the wear track lies between the arrows. The images on the right show higher magnification BSE images of the wear track surface, with an area in which WC grain pull-out has occurred circled.

the phase composition of the three coatings; ID110 was found to have a lower weight percentage of W_2C (4.68 wt%) and greater amounts of M_6C (8.19 wt%) in comparison to the other two coatings. The formation of η phase carbides has been shown to occur when a carbon deficiency exists at the hard phase – binder interface [17], suggesting that more carbon was oxidised out of the equilibrium melt during flight due to the greater stand-off distance leading to a greater M_6C composition in the ID110 coating. The greater weight composition of M_6C carbides found in ID110 in comparison to the other coatings may explain why this coating was found to have the lowest fracture toughness of the three coatings, as it has been shown that the increased presence of this phase worsens the mechanical properties of the material [18].

The specific wear rates of the three coatings and images of the wear tracks in Figs. 6–9 indicate that two different mechanisms of wear are occurring in the ID70/ID90 and ID110 coatings.

The ID70 96 N wear scar is characterised by cracks seen protruding along the entire width of the scar, accompanied by evidence of oxidised material. At the higher load, this oxidised material is visible in large amounts. A possible mechanism to explain what is occurring is as follows: due to the lower microhardness of the ID70 coating, material can more readily be broken off the surface when in contact with the counterbody. This debris is then oxidised due to the heat generated between the worn surface and counterbody and this oxidised material then remains in contact with the counterbody until it falls into the holes in the worn surface. As the load is increased, the effect is amplified due to the greater contact pressure leading to accelerated debris formation, heat generation and therefore oxidation. As the size of these oxidised sites is roughly in the range of that of one of more feedstock particles, it is likely the coating is breaking on a multi splat level. This may indicate a possible cohesion issue in this coating, meaning that delamination of individual or groups of splats is more easily induced when under load. Due to the short stand-off distance, it is likely that particles are still undergoing acceleration prior to impacting the substrate; this may explain why these issues are seen in the ID70 coating and not the other two.

At 96 N the main mechanism of wear for the ID90 sample appears to occur due the pull-out of the WC phase, as seen by other researchers [19]. The perimeter of the remaining holes are smooth edges of binder phase, characteristic of a brittle fracture. This suggests that for this sample the mechanism of wear was possibly dominated by brittle fracture of the binder. When the load was increased to 240 N, regions with larger areas of material pull-out can be observed. The existence of these areas could be due to the coalescing of cracks propagating through the brittle binder, greatly reducing the material toughness in these regions.

Alongside these regions, areas of the same brittle tribo-oxidation observed on the ID70 sample can be seen.

The friction coefficient of ID70 and ID90 was seen to increase to a peak value of almost 0.8; this did not happen in the other tests. These periods of increased friction coefficient may explain the increased

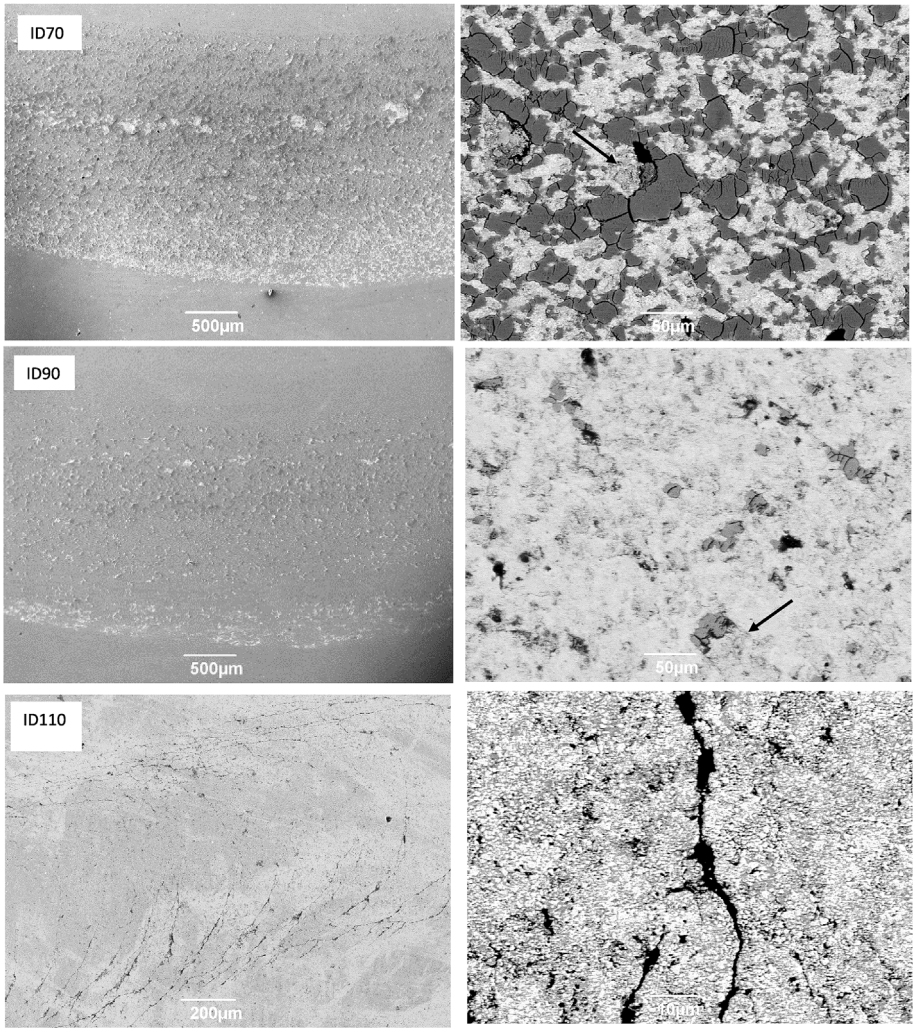

Fig. 8. Plan view SEM images of the wear scars produced from the sliding wear tests at 240 N for all three coatings. The images on the left column show low magnification SE images of the wear track and the image on the right column show higher magnification BSE images of the track. Areas in which brittle coating material has broken off have been marked with an arrow.

oxidised debris, as more energy will be converted into heat during these periods, increasing the oxidation rate of debris. As oxidised material was not found on the worn surfaces where this friction coefficient increase did not occur, then it is likely this may be the cause.

A smaller increase in specific wear rate was measured for ID110 when the load was raised from 96 N to 240 N, and SEM images of the wear tracks of this sample show the smallest difference in track width between the two loads. Parabolic shaped cracking is observed at the 240 N load, with the cracks propagating from within the track perpendicular to the counterbody movement to outside the track, parallel to the movement of the counterbody. This failure mode is characteristic of a buckling mechanism, in which the failure occurs due to the material's response to the compressive stresses generated ahead of the counterbody. Cracks are formed at the edge of the wear track due to the counterbody pushing the coating material outwards towards the edge of the track. Localised regions of the coating with interfacial defects provide areas in which the coating is allowed to buckle in response to these stresses [20], and these buckles can then spread by propagation of interfacial cracks. The high magnification SEM image in Fig. 8 shows crack propagation occurs preferentially around areas high in the WC phase, highlighting these areas as potential weak points. Although the specific wear rate of this coating at 240 N was found to be lower than that of the ID70, the way this coating has worn in response to these wear tests suggests that this coating may not currently be suitable for any practical application at higher loads.

Overall, ID70 performed worse than ID90 across both loads due to the increased microhardness and fracture toughness of the ID90 coating. ID110 was found to crack at both loads unlike the other coatings, due to having a reduced fracture toughness. From the results of this study, it appears that the fracture toughness of the coatings has a more dominant effect on the sliding wear resistance in comparison to microhardness, in particular at the 96 N load. This conclusion can be made due to the fact that while the microhardness of ID90 and ID110 was found to be very similar, the mechanism of wear and specific wear rate was very different. Visual evidence from the SEM images in Figs. 7 and 8 show that brittle fracture of the binder phase is the main cause of wear, regardless of whether individual WC grain pull-out or larger scale material pull-out is occurring. The lower fracture toughness of the ID110 resulted in increased crack propagation from the wear tests, in comparison to the other two samples, leading to the highest measured specific wear rate at 96 N. Meanwhile when increasing the load to 240 N the ID70 coating then suffered the most wear. This coating had the lowest microhardness of the three coatings, suggesting that at the high load the microhardness of the coating starts to become key.

The mechanical properties of the sprayed coatings and results from the dry sliding wear testing suggest that the most durable coating for a wear resistance application was ID90, suggesting that when using the selected spray parameters, spraying within an internal diameter of

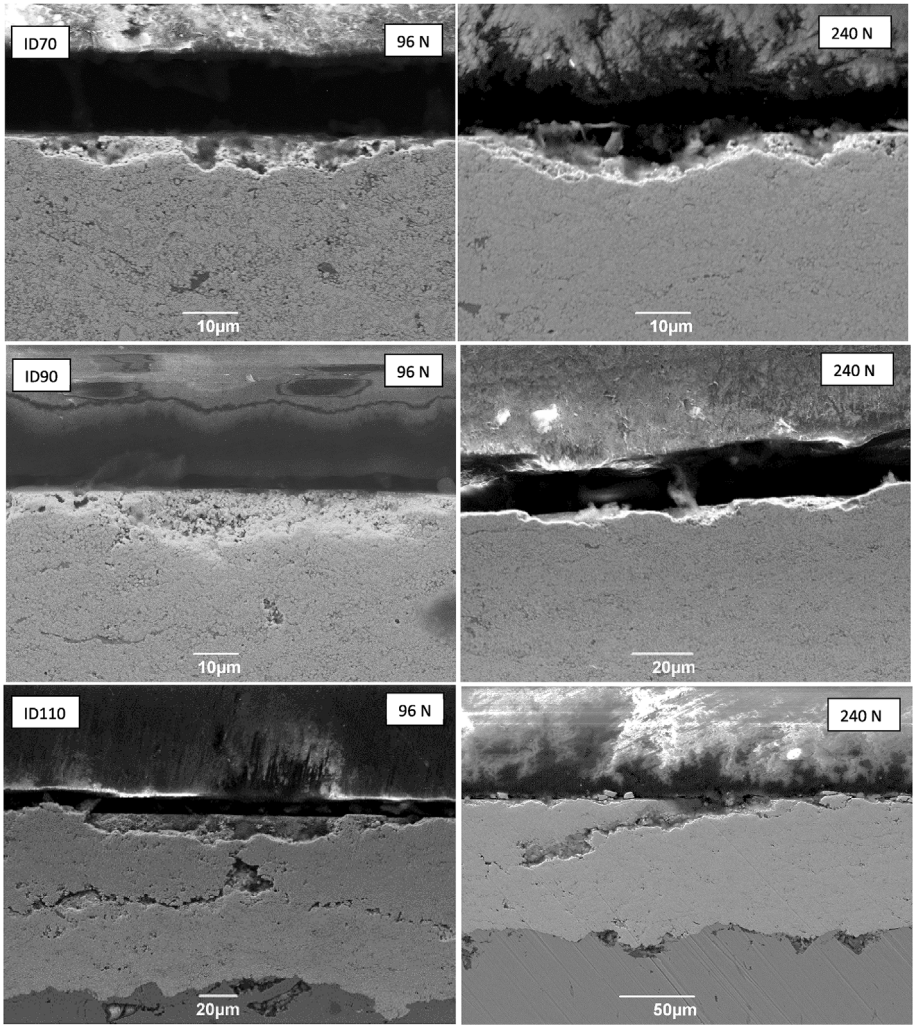

Fig. 9. SE SEM images showing the cross section of the wear scars produced from sliding wear testing at 96 N and 240 N.

90 mm provides the optimum stand-off distance of 50 mm. The ID70 coating was found to have the lowest microhardness and this may be due to the fact that when spraying at stand-off distances this small, particles are still undergoing acceleration and heating. The microhardness of WC-Co-Cr coatings has been shown to be influenced heavily by inflight particle properties, with slower particle velocities and lower temperatures often resulting in softer coatings [21,22]. At the other end of the scale, ID110 was found to have higher microhardness, but its fracture toughness was reduced in comparison to the other coatings. At higher stand-off distances, particles have a longer time to react with atmospheric gases at elevated temperature, leading to greater amounts of brittle η-carbides in the microstructure and overall lower fracture toughness.

For comparison, a similar WC-CoCr coating sprayed using commercially used parameters using a MetJet IV spray torch (Metallisation Ltd, UK) was subjected to dry sliding wear testing against a WC-Co counterbody using the same parameters as those used in this study at 96 N, and the sliding wear rate was determined to be 1.42×10^{-8} mm^3/Nm. This comparison suggests that the internally sprayed coatings will perhaps require further optimisation; nonetheless, the coatings presented here show excellent wear performance for small ID cylinders that are relevant to many high value engineering applications.

5. Conclusion

Three WC-10Co-4Cr coatings were sprayed using a compact HVOAF spray torch developed by Castolin-Eutectic Monitor Coatings Ltd, (UK) in a setup allowing for the simulation of coating the internal surface of a cylindrical pipe with internal diameter of 70 mm, 90 mm and 110 mm. The microstructure of the powders and coatings was analysed by SEM imaging and XRD analysis with Rietveld Refinement, with the mechanical properties and resistance to dry sliding wear measured as a performance metric.

The ID90 coating was found to possess the best mechanical properties of all coatings tested and, as a result, performed the best in the wear testing both at 96 N and at 240 N loads. The coating sprayed within the 70 mm ID was shown to perform better than the 110 mm ID at 96 N in the wear tests. However, further increasing the pipe internal diameter to 110 mm resulted in reduced fracture toughness of the coating and higher wear rate at both loads. This confirms that, when using the spray parameters utilised in this study, a stand-off distance of 50 mm, appears to provide the optimum to obtain the best mechanical and wear performance. Particles sprayed at the lower stand-off distance may not reach the optimal velocity for impact, meanwhile those sprayed in the larger sized ID were exposed to high temperatures for a longer period, leading to a more brittle coating.

The results in this paper indicate that WC-Co-Cr powder from a commercial feedstock can be deposited on internal surfaces by the HVOF process, producing a coating without large defects. However it has been shown that using the same spray parameters when spraying all three different IDs may not be optimal, as the mechanical properties of the coating were worse for the ID70 and ID110 coatings, which was

seen to affect the tribological performance. Wear rate at 96 N was seen to be largely affected by the fracture toughness of the coatings, with the most brittle sample (ID110) expressing the highest wear. When load was increased to 240 N, the sample sprayed at the shortest stand-off distance was found to wear the most due to its low microhardness. Specific parameter optimisation when spraying each separate ID may be required to improve the mechanical properties and therefore the wear resistance for each coating in order to further improve their tribological performance.

Acknowledgement

This work was supported by the Engineering and Physical Sciences Research Council [EP/L016362/1]; in the form of an EngD studentship and industrial funding from Castolin Eutectic- Monitor Coatings Ltd.

References

[1] J. Picas, M. Punset, M. Teresa Baile, E. Martín, A. Forn, Tribological evaluation of HVOF thermal-spray coatings as a hard chrome replacement, Surf. Interface Anal. 43 (10) (2010) 1346–1353.
[2] T. Gong, P. Yao, X. Zuo, Z. Zhang, Y. Xiao, L. Zhao, et al., Influence of WC carbide particle size on the microstructure and abrasive wear behavior of WC–10Co–4Cr coatings for aircraft landing gear, Wear 362–363 (2016) 135–145.
[3] P. Fauchais, J. Heberlein, M. Boulos, Thermal Spray Fundamentals from Powder to Part, Springer, New York, 2014.
[4] B. Allcock, P. Lavin, Novel composite coating technology in primary and conversion industry applications, Surf. Coat. Technol. 163–164 (2003) 62–66.
[5] C. Lyphout, S. Bjorklund, Internal diameter HVAF spraying for wear and corrosion applications, J. Therm. Spray Technol. 24 (2015) 235–243.
[6] L. Zhao, M. Maurer, F. Fischer, R. Dicks, E. Lugscheider, Influence of spray parameters on the particle in-flight properties and the properties of HVOF coating of WC-CoCr, Wear 257 (1–2) (2004) 41–46.
[7] W. Lih, S. Yang, C. Su, S. Huang, I. Hsu, M. Leu, Effects of process parameters on molten particle speed and surface temperature and the properties of HVOF CrC/NiCr coatings, Surf. Coat. Technol. 133–134 (2000) 54–60.
[8] V. Katranidis, S. Gu, B. Allcock, S. Kamnis, Experimental study of high velocity oxy-fuel sprayed WC-17Co coatings applied on complex geometries. Part A: influence of kinematic spray parameters on thickness, porosity, residual stresses and micro-hardness, Surf. Coat. Technol. 311 (2017) 206–215.
[9] S. Gu, S. Kamnis, Bonding mechanism from the impact of thermally sprayed solid particles, Metall. Mater. Trans. A 40 (11) (2009) 2664–2674.
[10] J. Pulsford, S. Kamnis, J. Murray, M. Bai, T. Hussain, Effect of particle and carbide grain sizes on a HVOAF WC-Co-Cr coating for the future application on internal surfaces: microstructure and wear, J. Therm. Spray Technol. 27 (1–2) (2017) 207–219.
[11] B. Kear, G. Skandan, R. Sadangi, Factors controlling decarburization in HVOF sprayed nano-WC/Co hardcoatings, Scr. Mater. 44 (8–9) (2001) 1703–1707.
[12] S. Gu, S. Kamnis, Numerical modelling of in-flight particle dynamics of non-spherical powder, Surf. Coat. Technol. 203 (22) (2009) 3485–3490.
[13] B. Allcock, S. Gu, S. Kamnis, Nozzle for a Thermal Spray Gun and Method of Thermal Spraying, (2013), p. EP2411554A.
[14] ASTM G99-17, Standard Test Method for Wear Testing with a Pin-on-Disk Apparatus, ASTM International, West Conshohocken, PA, 2017.
[15] A.G. Evans, T.R. Wilshaw, Quasi-static solid particle damage in brittle solids—I. Observations analysis and implications, Acta Metall. 24 (10) (1976) 939–956.
[16] C. Verdon, A. Karimi, J. Martin, A study of high velocity oxy-fuel thermally sprayed tungsten carbide based coatings. Part 1: Microstructures, Mater. Sci. Eng. A 246 (1–2) (1998) 11–24.
[17] L.M. Berger, P. Ettmayer, P. Vuoristo, T. Mäntylä, W. Kunert, Microstructure and properties of WC-10%Co-4% Cr spray powders and coatings: Part 1. Powder characterization, J. Therm. Spray Technol. 10 (2) (2001) 311–325.
[18] G. Lee, S. Kang, Sintering of nano-sized WC–Co powders produced by a gas reduction–carburization process, J. Alloy. Comp. 419 (1–2) (2006) 281–289.
[19] T. Sudaprasert, P. Shipway, D. McCartney, Sliding wear behaviour of HVOF sprayed WC–Co coatings deposited with both gas-fuelled and liquid-fuelled systems, Wear 255 (7–12) (2003) 943–949.
[20] S. Bull, Failure mode maps in the thin film scratch adhesion test, Tribol. Int. 30 (7) (1997) 491–498.
[21] X. Guo, M. Planche, J. Chen, H. Liao, Relationships between in-flight particle characteristics and properties of HVOF sprayed WC-CoCr coatings, J. Mater. Process. Technol. 214 (2) (2014) 456–461.
[22] J.A. Picas, M. Punset, M.T. Baile, E. Martín, A. Forn, Effect of oxygen/fuel ratio on the in-flight particle parameters and properties of HVOF WC-CoCr coatings, Surf. Coat. Technol. 205 (2011) S364–S368.